RSC Advances

ROYAL SOCIETY OF CHEMISTRY

www.rsc.org/advances

RSC Advances

RSC Advances

Dynamic Article Links ►

Cite this: DOI: 10.1039/c0xx00000x

www.rsc.org/xxxxxx

ARTICLE TYPE

Highly luminescent lanthanide fluoride nanoparticles functionalized by aromatic carboxylates acid

Suwen Li,[a] Xuejiao Li,[b] Yi Jiang,[a] Zhiyao Hou,[b] Ziyong Cheng,[b] Pingan Ma,[b] Chunxia Li[b] and Jun Lin*[b]

Received (in XXX, XXX) Xth XXXXXXXXX 20XX, Accepted Xth XXXXXXXXX 20XX
DOI: 10.1039/b000000x

The highly dispersible LaF_3: x%Tb^{3+} (x = 1, 3, 5, 8, 10) nanoparticles capped with citrate ligands have been prepared and functionalized by salicylate and 5-sulfosalicylate, respectively. The structure, morphology, photoluminescence properties, fluorescence dynamics and ligand sensitization mechanism have been studied systemically. Monitoring the characteristic emission of the Tb^{3+} $^5D_4$ – $^7F_5$ transition, the broad absorption bands in the UV domain are obtained in the functionalized nanoparticles. Under excitation of the $\pi - \pi^*$ electron transition absorption of salicylate (or 5-sulfosalicylate), the enhanced luminescence of Tb^{3+} ions is achieved in the functionalized nanoparticles. The ligand sensitization is potentially interpreted by a dipole – dipole sensitization mechanism. The luminescence lifetimes of Tb^{3+} ions in the nanoparticles functionalized by aromatic carboxylates acid are longer than ones in LaF_3: Tb^{3+} nanoparticles capped with citrate ligands.

Introduction

Fluoride is a kind of ideal host material for the luminescent lanthanide ions (Ln^{3+}). This is due to its low phonon energy (~300 cm^{-1} for LaF_3) and small multi-phonon relaxation rate, which could in principle reduce the luminescence quenching and lead to higher luminescent efficiency and longer luminescent lifetimes for the lanthanide ions. Furthermore, fluorides exhibit thermal and environmental stability as well as large solubility for lanthanide ions. Therefore, they possess promising applications in lighting, displays, biological labels, bioprobe and optical amplifies.[1] However, fluorides doped with lanthanide ions also have intrinsic limit that is no absorbance in the UV range in practical application. Specially, luminescence of Ln^{3+} originates from electronic transitions between the 4f orbital and these transitions are strongly forbidden by the parity selection rules, which lead to low molar absorption coefficients ($\varepsilon = 1 - 10$ M^{-1} cm^{-1})[2] associated with 4f → 4f transitions and narrow absorption band, which leads to inefficient optical excitation and low luminescence intensity. To overcome these disadvantages, sensitizers are usually used for efficiently absorbing and transferring the energy to the lanthanide ions. Sensitizers mainly include organic sensitizers and inorganic sensitizers. The organic sensitizers are usually employed in lanthanide complexes, which often called the "antenna effect". However, the lanthanide complexes have certain shortcoming such as poor optical, thermal, chemical stabilities and short lifetimes in practical applications. The inorganic sensitizers usually sensitize luminescence of lanthanide ions doped in nanoparticles, such as semiconductor[3,4] and vanadate host materials,[5,6] Ce^{3+} ions[7-10] and Yb^{3+} ions[11,12] as co-dopants of luminescence center ions. The inorganic host materials can protect lanthanide cations from sources of nonradiative deactivation, but they have either limit or no absorbance in the UV range.[13]

Recently, most of the studies on lanthanide doped phosphors have been focused on inorganic luminescence composite functionalized by organic ligands, i.e. organic ligands as sensitizers for 4f → 4f emission of Ln^{3+} ions are bonded onto the surface of nanoparticles doped Ln^{3+} ions.[13-23] Briefly, the excitation wavelength used is in resonance with a strong ligands absorbance. Then excited ligands efficiently transfer its energy to the Ln^{3+} ions and achieve efficient emission. At the same time, the inorganic matrix protects lanthanide ions from sources of nonradiative deactivation and can provide high quantum yields and superior photostability. Aromatic carboxylate, owning great optical absorption coefficients in the UV area, is a kind of important sensitizer for luminescent lanthanide ions. The researches on that aromatic carboxylates sensitize luminescence of lanthanide ions doped in nanoparticles are rarely reported.

Herein, in this work, the water dispersible, citrate stabilized, small-sized LaF_3:Tb^{3+} nanoparticles are prepared by a low temperature synthesis route, and sensitized by salicylate (SA) 5-sulfosalicylate (SSA) bonded on surface of nanoparticles, respectively. The structure, morphologies, photoluminescence (PL) properties and fluorescence dynamics of these nanoparticles have been investigated in detail.

Experimental section

Chemicals and Materials

The rare earth oxides La_2O_3 and Tb_4O_7 (99.999%) were purchased from Science and Technology Parent Company of Changchun Institute of Applied Chemistry, and other chemicals were purchased from Beijing Chemical Company. All chemicals

are of analytical grade reagents and used directly without further purification.

Preparation of citrate capped-LaF_3: Tb^{3+} nanoparticles

The LaF_3: x%Tb^{3+} (x = 1, 3, 5, 8, 10) nanoparticles were prepared according to ref 2 and 15. In a typical experiment, 0.65 mmol of La_2O_3 and stoichiometric Tb_4O_7 were dissolved in concentrated HNO_3 firstly by stirring the mixture at about 90 ^oC until crystal growed, and then 2 ml of methanol was added to form transparent lanthanide nitrate methanol solution. An aqueous solution of 10.4 mmol of citric acid was added into 35 ml of deionized water. Then nitrate methanol solution was added dropwise to the citric acid aqueous solution. The appropriate amounts of NaF aqueous solution then was added under stirring. The reaction mixture was further stirred for 2 h at 75 °C and then allowed to cool to room temperature. The resulted nanoparticles were precipitated by adding ethanol and separated from the suspension by centrifugation. The precipitates were washed by ethanol and dried in vacuum overnight.

Preparation of surface functionalized nanoparticles

Appropriate amounts of sodium salicylate (or sodium 5-sulfosalicylate) were added into 40 ml of deionized water. The transparent SA (or SSA) aqueous solution was obtained under strong stirring. The above obtained LaF_3: x% Tb^{3+} (x = 1, 3, 5, 8, 10) nanoparticles were uniformly dispersed into deionized water, and then added into the SA (or SSA) aqueous solution. The mixture was kept at 60 ^oC (65 ^oC for SSA) for 4 h under water bath backflow. The resulted products were separated by centrifugation. The as-separated products were washed by deionized water and dried in vacuum for 24 h. The obtained functionalized samples are labeled as SA- LaF_3: x% Tb^{3+} (x = 1, 3, 5, 8, 10) and SSA- LaF_3: x% Tb^{3+} (x = 1, 3, 5, 8, 10), respectively.

Preparation and functionalization of core – shell nanoparticles

In order to study the sensitization mechanism, the core – shell nanopaticles LaF_3:8%Tb^{3+}@LaF_3, LaF_3: 8%Tb^{3+}@ LaF_3@ LaF_3, LaF_3:5%Tb^{3+}@LaF_3, LaF_3:10% Tb^{3+}@LaF_3 and LaF_3:5%Tb^{3+}@ LaF_3:5%Tb^{3+} were prepared and functionalized by SA and SSA, respectively. In a typical experiment, 0.65 mmol of La_2O_3 and stoichiometric Tb_4O_7 were dissolved in concentrated HNO_3 firstly by stirring the mixture at about 90 ^oC until crystal grown, and then 2 ml of methanol was added, resulting the formation of transparent lanthanide nitrate methanol solution. Then the lanthanide nitrate methanol solution is added into the 35 ml of citric acid aqueous solution. The 8.2 mmol (12.3 mmol for double LaF_3 shell) of NaF aqueous solution was then added under stirring. The reaction mixture was further stirred for 2 h at 75 °C. Then the 1.3 mmol of lanthanide nitrate methanol solution was added and kept at 75 °C for 2 h, and then allowed to cool to room temperature. The resulted core-shell nanoparticles were precipitated by adding ethanol. The precipitate was washed by ethanol and dried in vacuum for 24 h. The obtained core – shell nanoparticles were functionalized as described prevuiously for the functionalization LaF_3: x% Tb^{3+} (x = 1, 3, 5, 8, 10) nanoparticles.

Characterizations

The X-ray diffraction (XRD) measurements were performed on a D8 Focus diffractometer (Bruker) with Cu Kα radiation (λ = 0.15405 nm). Fourier transform infrared (FTIR) spectra were recorded on a Perkin-Elmer 580B IR spectrophotometer in KBr pellets. The UV-vis absorption spectra were measured on a U-3310 scanning spectrophotometer. Transmission electron microscopy (TEM) and high-resolution transmission electron microscopy (HRTEM) images were obtained with an FEI Tecnai G2 S–Twin transmission electron microscopy with a field emission gun operated at 200 kV. The photoluminescence measurements were performed on a Hitachi F – 7000 spectrophotometer equipped with a 150 W xenon lamp as the excitation source. The luminescence decay curves were obtained from a Lecroy Wave Runner 6100 digital oscilloscope (1 GHz) by using a tunable laser (pulse width = 4 ns) as excitation source (Continuum Sunlite OPO). All measurements were performed at room temperature.

Results and discussion

Structure

The representative XRD pattern of LaF_3: 8%Tb^{3+}, SA sensitized LaF_3: 8%Tb^{3+}, SSA sensitized LaF_3: 8%Tb^{3+} (c) samples and the standard LaF_3 tysonite structure (ICDD 82-0690) were shown in Figure 1. All diffraction peaks of the samples can be readily indexed to pure tysonite of LaF_3 and the impurity phases do not appear in all samples. The structure of sensitized nanoparticles does not change compared with ones of un-sensitized nanoparticles. Moreover, the corresponding diffraction peaks of the all samples were markedly broadened and partly overlapped, indicating that the size of the as-obtained particles become very small.

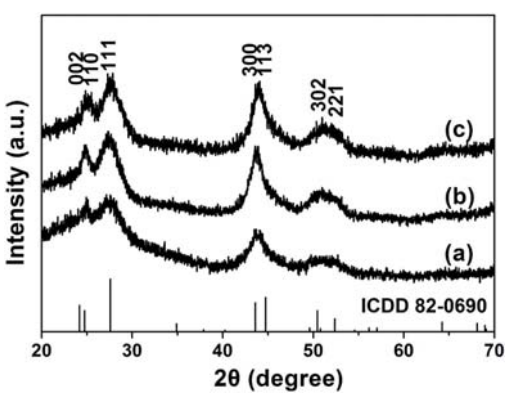

Figure 1 XRD patterns of LaF_3: 8%Tb^{3+} (a), SA sensitized LaF_3: 8%Tb^{3+} (b), SSA sensitized LaF_3: 8%Tb^{3+} (c) samples and the standard LaF_3 tysonite structure (ICDD 82-0690).

The average crystalline size of the samples can be estimated by the Scherrer formula, $D = K\lambda/\beta\cos\theta$, where D is the average particle size, λ is the X-ray wavelength (0.15405 nm), β is the full-width at half-maximum, θ is the diffraction angle of an observed peak, K is a constant (0.89), respectively. The estimated average crystallite size is about 3.28 nm for LaF_3: 8%Tb^{3+} samples, 3.32 nm for SA sensitized LaF_3: 8%Tb^{3+} samples and

3.35 nm for SSA sensitized LaF_3: 8%Tb^{3+} samples. The phase structures of the other concentration doped samples were examined by XRD in the same way. The results are in agreement with those of LaF_3: 8%Tb^{3+} and will not be shown here.

Morphologies

The morphologies of the obtained samples were characterized by TEM and HRTEM. The representative TEM image of LaF_3: 8%Tb^{3+} sample is shown Figure 2(a). For other doping concentrations of Tb^{3+} in the LaF_3: x%Tb^{3+} (x = 1, 3, 5, 10) and sensitized samples by SA and SSA, the results are similar to those of LaF_3: 8%Tb^{3+} and will not be shown here. From Figure 2(a), it can be seen that the obtained nanoparticles are roughly spherical and monodisperse. The illustration of Figure 2(a) shows the representative HRTEM image of LaF_3: 8%Tb^{3+} nanoparticles, which clearly reveals the well-resolved diffraction fringes of the lattices. It shows that the nanoparticles are perfect crystalline. The lattice fringes with 0.226 nm spacing are clearly visible and in accordance with the lattice spacing of (1 2 1) of LaF_3 crystal. The Figure 2(b) shows the statistics of diameter distribution of the nanoparticles for the representative of LaF_3: 8%Tb^{3+} sample. The mean diameter of the nanoparticles is 3.25 nm (the total particles reach to 100) and the nanoparticles size distribution is narrow. It is approximately consistent with the results of XRD.

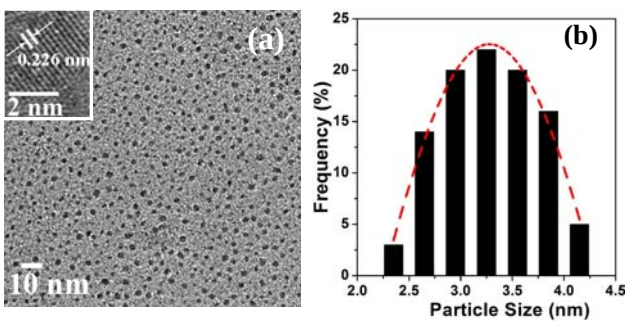

Figure 2 (a) TEM images of LaF_3: 8% Tb^{3+} samples, inset: HRTEM images of LaF_3: 8% Tb^{3+} samples, (b) histogram of diameter distribution of the nanoparticles.

FTIR

Figure 3(a) shows the FTIR absorption spectra of NaSA and SA-LaF_3: x%Tb^{3+} (x = 1, 3, 5, 8, 10) samples. Comparing the FTIR spectra of functionalized samples with those free of sensitizer, remarkable differences can be seen. The antisymmetry stretching vibration (ν_{as}coo-) peak and the stretching vibration ($\nu_s$coo-) peak for carboxyl shift from 1578 cm^{-1} (for SA) to 1588 cm^{-1} and from 1375 cm^{-1} (for SA) to 1408 cm^{-1}, respectively. The $\Delta\nu$ decreases from 203 cm^{-1} to 180 cm^{-1}, implying that the carboxyls of the NaSA, as acid radical, coordinate with the lanthanide ions located on the surface of nanoparticles. Furthermore, the in-plane deformation vibration of phenolic hydroxyl (δ_{O-H}) at 1485 cm^{-1} and 1466 cm^{-1} disappear. The stretching vibration of phenolic hydroxyl (Ar-OH) shifts from 1299 cm^{-1} to 1263 cm^{-1} ($\Delta\nu$ = 36 cm^{-1}). These changes show that the phenolic hydroxyl in the NaSA coordinate with the lanthanide ions located on the surface of nanoparticles, too. The coordination mode will be further studied. Figure 3(b) shows the FTIR absorption spectra of NaSSA and SSA- LaF_3: x%Tb^{3+} (x = 1, 3, 5, 8, 10). The FTIR spectra of functionalized samples and free ligands are obviously different. For SSA- LaF_3: x%Tb^{3+} (x = 1, 3, 5, 8, 10) samples, the absorption peak of carboxycarbonyl (C = O) at 1671 cm^{-1} disappears. At the same time the antisymmetry stretching vibration (ν_{as}coo-) at 1589 cm^{-1} and the stretching vibration ($\nu_s$coo-) at 1404 cm^{-1} for carboxyl appear. In addition, vibration absorption of phenolic hydroxyl (δ_{O-H}) at 1477 cm^{-1} and 1436 cm^{-1} disappear. The stretching vibration of phenolic hydroxyl (Ar-OH) shifts from 1306 cm^{-1} to 1260 cm^{-1} ($\Delta\nu$ = 46 cm^{-1}). It overlaps with characteristic vibration of sulfonyl at 1225 cm^{-1}. These results show that not only carboxyl but phenolic hydroxyl coordinates with the lanthanide ions located on the surface of nanoparticles. The absorption of sulfonyl at 1225 cm^{-1}, 1168 cm^{-1} and 1036 cm^{-1} almost do not change, which indicate that the sulfonyl does not participate in coordination.

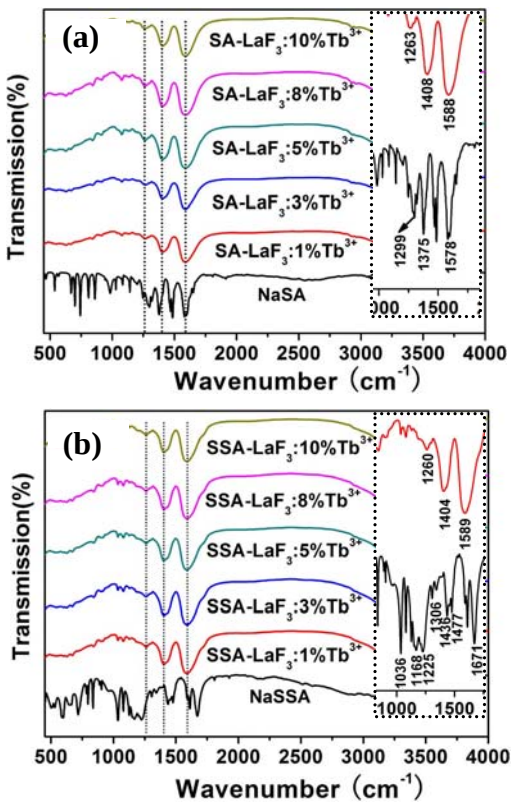

Figure 3 FTIR spectra of NaSA and SA- LaF_3: x%Tb^{3+} (x =1, 3, 5, 8, 10) (a), NaSSA and SSA- LaF_3: x%Tb^{3+} (x =1, 3, 5, 8, 10) (b).

UV-Vis absorption

UV-vis absorption spectra of NaSA and SA- LaF_3: x%Tb^{3+} (x =1, 3, 5, 8, 10) are drawn in Figure 4(a). Three absorption bands located around 204 nm, 228 nm and 295 nm can be observed, corresponding to the $\pi - \pi^*$ transition of the salicylic ligands. This implies that three different excitation state energies at least exist in the salicylic ligand. In contrast to NaSA, the shapes of the three bands are same and their locations are slightly red-shift in SA- LaF_3: x%Tb^{3+} (x =1, 3, 5, 8, 10). This is because the conjugation of ligands is decreased after coordination of SA with rare earth ions on the surface of nanopaticles. In the Figure 4(b) UV-vis absorption spectra of NaSSA and SSA- LaF_3: x%Tb^{3+} (x =1, 3, 5, 8, 10) are shown. The three absorption bands at 207 nm, 235 nm and 298 nm are corresponding to the $\pi - \pi^*$ transitions of

the sulfosalicylic ligands, implying that three different excitation state energies exist in the sulfosalicylic ligand at least. The shapes of the three bands are identical with those of NaSSA. The imperceptible red-shifts are detected for the three bands in the SSA- LaF_3: x%Tb^{3+} (x =1, 3, 5, 8, 10) samples, which can be attributed to the variation of conjugated degree for ligands participated coordination.

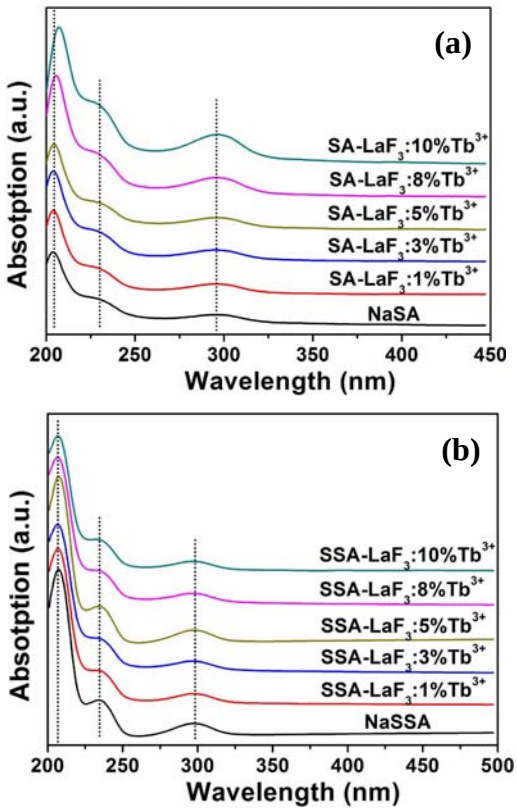

Figure 4 UV-vis absorption spectra of NaSA and SA- LaF_3: x%Tb^{3+} (x =1, 3, 5, 8, 10) (a), NaSSA and SSA- LaF_3: x%Tb^{3+} (x =1, 3, 5, 8, 10) (b).

Photoluminescence properties

To determine the sensitized effect for luminescence of Tb^{3+} doped in LaF_3 nanoparticles by the aromatic carboxylates (SA and SSA), the photoluminescence spectra of LaF_3: x%Tb^{3+} (x = 1, 3, 5, 8, 10) samples with and without functionalization by the aromatic carboxylates were measured at room temperature, as shown in Figure 5. Figure 5(a) gives the excitation and emission spectra of LaF_3: x%Tb^{3+} (x = 1, 3, 5, 8, 10) samples without functionalization. The excitation spectra (left of Figure 5(a)) were obtained by monitoring the emission of the Tb^{3+} $^5D_4$ – $^7F_5$ transition at 547 nm. The excitation spectra consist of the characteristic the $4f^8$ – $4f^75d$ transitions and forbidden f – f transitions within the Tb^{3+} $4f^8$ configuration of the Tb^{3+} ions. The excitation band centered at 233 nm is attributed to the spin-allowed ($\triangle S = 0$) components of the transitions from the $^7F_6$ ground state of the $4f^8$ configuration to the excited-state of the $4f^75d$ configuration of the Tb^{3+} ions.[24] The excitation bands from 280 nm to 400 nm can be assigned to the transitions from the $^7F_6$ ground state to the different excited states.[25] The shape of the excitation spectra and peaks position in the samples with different doping concentration are similar. Upon excitation of the $^7F_6 \rightarrow {}^5D_3$ transition at 378 nm, the obtained emission spectra are shown in right of Figure 5(a). It is obvious that the shapes of the spectra and peaks position in the samples with different concentration of Tb^{3+} are similar. The emission spectra show three obvious bands centered at 492, 547 and 587 nm, originating from the transitions from the $^5D_4$ excited state to the ^7F_J (J = 4, 5, 6) ground states of the Tb^{3+} ion respectively, with the $^5D_4 \rightarrow {}^7F_5$ transition at 547 nm as the most prominent group. The emission intensity increases with increasing Tb^{3+} concentration up to 8%. The quenching concentration in small sized nanoparticles is higher than those in the bulk materials because of the reduction of energy transfer rate from luminescence centers to quenching centers by the interface effect.[26]

The excitation and emission spectra of LaF_3: x%Tb^{3+} (x = 1, 3, 5, 8, 10) nanoparticles functionalized by SA are detected at room temperature and depicted in right of Figure 5(b). Monitoring the $^5D_4 \rightarrow {}^7F_5$ transition of Tb^{3+} at 545 nm, the excitation spectra are composed of a broad and intense excitation band from 200 nm to 375 nm, due to the $\pi - \pi^*$ electron transition of the SA ligands, with some weak characteristic absorption bands of Tb^{3+}. This fully proves that the Tb^{3+} in LaF_3 nanoparticles is excited by the organic ligand SA through the "antenna" effect. Upon the excitation of $\pi - \pi^*$ electron transition of the SA ligands at 312 nm, the obtained emission spectra of the samples are shown in right of Figure 5(b). The shape and emission peak position of the spectra in the samples with different doping concentration of Tb^{3+} are similar. The intense, characteristic green emission bands of Tb^{3+} are observed, corresponding to the $^5D_4 \rightarrow {}^7F_J$ (J = 4, 5, 6) transitions. The strongest emission at 545 nm corresponds to the hypersensitive $^5D_4 \rightarrow {}^7F_5$ transition. The inset of Figure 5(b) is luminescence photographs of SA- LaF_3: 8% Tb^{3+} nanoparticles in aqueous solution under 254 nm UV light excitation. The luminescence of corresponding powder nanopaticles under 254 nm UV light can also be observed (the photographs are not shown here). All un-sensitized samples do not show any luminescence under 254 nm UV light excitation. The results further confirm that SA can effectively sensitize the luminescence of Tb^{3+} in LaF_3 nanoparticles.

Figure 5(c) show the excitation and emission spectra of the functionalized LaF_3: x%Tb^{3+} (x = 1, 3, 5, 8, 10) nanoparticles by SSA. Monitoring the Tb^{3+} characteristic emission at 545 nm at room temperature, the excitation spectra of SSA- LaF_3: x % Tb^{3+} (x = 1, 3, 5, 8, 10) nanoparticles are detected and drawn in the left of Figure 5(c). A broad excitation band ranging from 200 to 380 nm assigned to the $\pi - \pi^*$ electron transition of the SSA ligands can be seen. This indicates that the Tb^{3+} in LaF_3 nanoparticles is excited by the SSA ligands through the "antenna" effect. Upon excitation of $\pi - \pi^*$ electron transition of the SA ligands at 320 nm, the emission spectra clearly show strong characteristic Tb^{3+} emission bands in the green wavelength region (located right of Figure 5(c)), originating from the $^5D_4 \rightarrow {}^7F_J$ (J = 4, 5, 6) transitions of Tb^{3+} ions. The shape and emission peak position of the spectra in the samples with different concentration are similar. The inset of Figure 5(c) is luminescence photographs of SSA- LaF_3: 8% Tb^{3+} powder sample in a copper groove under 254 nm UV light excitation. All un-sensitized samples do not show luminescence under 254 nm UV light excitation. The results farther prove that SSA can effectively sensitize the luminescence

of Tb^{3+} in LaF_3 nanoparticles. The luminescence photographs of SSA- LaF_3: 8% Tb^{3+} nanoparticles in aqueous solution under 254 nm UV light excitation are similar to that of SA- LaF_3: 8% Tb^{3+} and will not be repeatedly shown here.

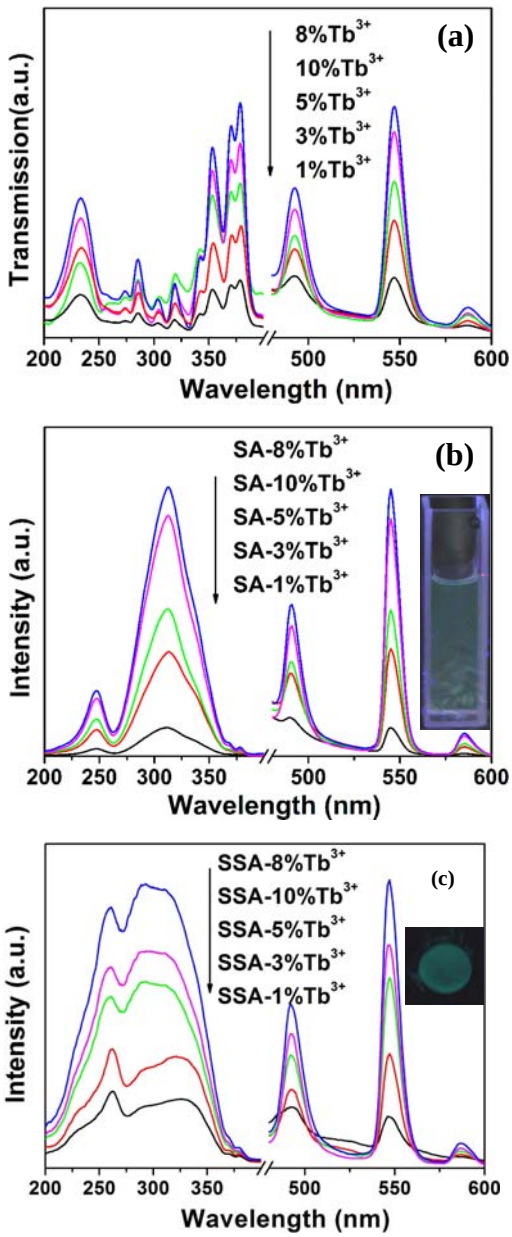

Figure 5 excitation and emission spectra of LaF_3: x% Tb^{3+} (x =1, 3, 5, 8, 10) nanopaticles (a), SA-LaF_3: x% Tb^{3+} (x =1, 3, 5, 8, 10) (b) and SSA- LaF_3: x%Tb^{3+} (x =1, 3, 5, 8, 10) (c). The insets are the luminescence photographs of SA- LaF_3: 8% Tb^{3+} nanoparticles in aqueous solution (b) and the luminescence photographs of SSA- LaF_3: 8% Tb^{3+} nanoparticles (c) under 254 nm UV light excitation, respectively.

The schematic energy level diagram of SA (or SSA) with Tb^{3+} levels is shown in Figure 6. The energy transfer pathway in the SA (or SSA)-LaF_3: Tb^{3+} nanoparticles generally consists of an initial strong absorption of ultraviolet energy that excites SA (or SSA) to the excited singlet (S_1) state, followed by an energy migration via intersystem crossing from the S_1 state to a SA (or SSA) triplet (T) state. The energy is then nonradiatively transferred from the lowest triplet state of SA (or SSA) to a resonance state of a coordinated Tb^{3+} ion, which in turn undergoes a multiphoton relaxation and subsequent emission in the visible region.

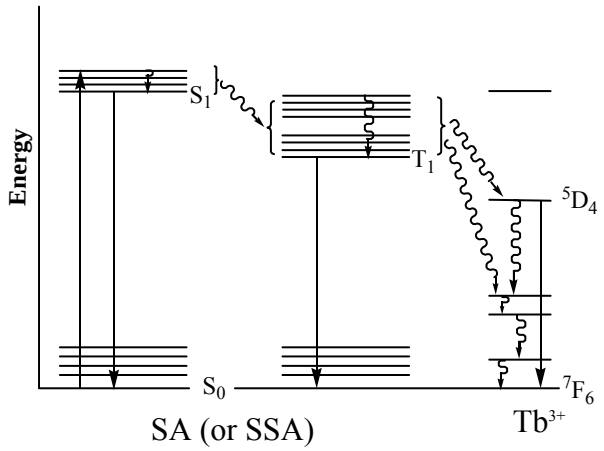

Figure 6 Schematic energy level diagram of SA (or SSA) with Tb^{3+} levels. S_0: ground state of SA (or SSA), S_1: excited singlet state of SA (or SSA), T_1: excited triplet state of SA (or SSA), $^5D_4$ and $^7F_6$: Tb^{3+} ion excited and ground state energy levels, respectively. straight arrow: radiative transition, curve arrow: noradiative transition.

It is well known that the ligand sensitization is known as a short-range effect. The occurred mechanism is referred to (I) an electron exchange mechanism effecting only when the ligand is directly coordinated to the Ln^{3+} ion or (II) a dipole – dipole mechanism. The energy transfer efficiency (η) reducing with increasing separation distance (R) between donor and acceptor can be written as

$$\eta = 1/\left(1+\left(R/R_0\right)^6\right) \qquad (1)$$

where R_0 is a Förster constant and the typical values are in the range of 5 - 20 Å.[15] The sensitization mechanism of SA and SSA for Tb^{3+} in LaF_3 nanoparticles is studied. It is can be tested by comparing the luminescence properties of LaF_3: x% Tb^{3+} (x = 1, 3, 5, 8, 10) nanoparticles with and without a encapsulating LaF_3 shell. The core-shell nanoparticles were prepared as described in the experimental section, and the shell with thick about 0.4 nm was obtained as confirmed by Cross et al.[15] The representative emission spectra of LaF_3: 8%Tb^{3+} core, LaF_3: 8%Tb^{3+} core @LaF_3 shell and LaF_3: 8%Tb^{3+} core@ double LaF_3 shell sensitized by SA (or SSA) were detected and shown in Figure 7, respectively.

It is distinct that the addition of a LaF_3 shell decreases the emission intensity of Tb^{3+} to about 25% of the original, implying that the efficiency of the SA (or SSA) ligands sensitization reduces due to the shell having dramatically increased the distance of Tb^{3+} ions located on the surface sites and the SA (or SSA) ligands. The emission intensity of Tb^{3+} further decreases in the double thickness LaF_3 shell, but the sensitization effect of SA (or SSA) for Tb^{3+} ions still exist. Notably, above comparisons of emission spectra between the core and core@shell are obtained

on this condition that the core and core@shell nanoparticls are of different sizes. The shell with thick about 0.4 nm increases size of nannoparticles and the influence of size effects on luminescence also must be considered as well. Therefore, the luminescence of nanoparticles with the same size and same net Tb^{3+} concentration are compared. The LaF_3: 10%Tb^{3+} core @ LaF_3 shell, LaF_3: 5%Tb^{3+} core @ LaF_3: 5%Tb^{3+} shell and LaF_3: 5%Tb^{3+} core @ LaF_3 shell nanoparticles were prepared and functionalized by SA (or SSA).

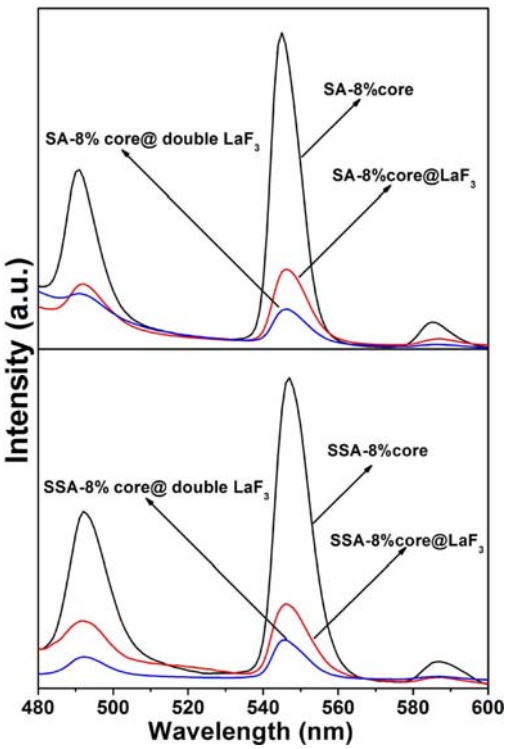

Figure 7 Emission spectra of SA-LaF_3: 8%Tb^{3+} core, SA-LaF_3: 8%Tb^{3+} core @LaF_3 shell, SA-LaF_3: 8%Tb^{3+} core@ double LaF_3 shell, SSA-LaF_3: 8%Tb^{3+} core, SSA-LaF_3: 8%Tb^{3+} core @LaF_3 shell and SSA-LaF_3: 8%Tb^{3+} core@ double LaF_3 shell.

The emission spectra of these sensitized samples were detected and drawn in Figure 8. Compared to LaF_3: 5%Tb^{3+} core @ LaF_3: 5%Tb^{3+} shell, the SA (or SSA) sensitization for the LaF_3: 10%Tb^{3+} core @ LaF_3 shell is reduced to 25% of the original one. This demonstrates that the Tb^{3+} dopant are not fully equilibrated throughout the nanoparticles, and that a distinct core-shell structure falls off the energy transfer efficiency from ligands to luminescent center ions. The fact that the shell does not more effectively block the sensitization than the observed 75% diminution is potentially interpreted by a dipole – dipole sensitization mechanism as described in eq 1. The distance R in eq 1 is measured from the center of the SA (or SSA) ring to the center of a Tb^{3+} at the surface and the result is about 5 Å, the addition of shell with 4 Å thickness will lead to that the efficiency η fall off by a factor of 4, with R_0 falling in the physically reasonable range of 7 - 8 Å.[15]

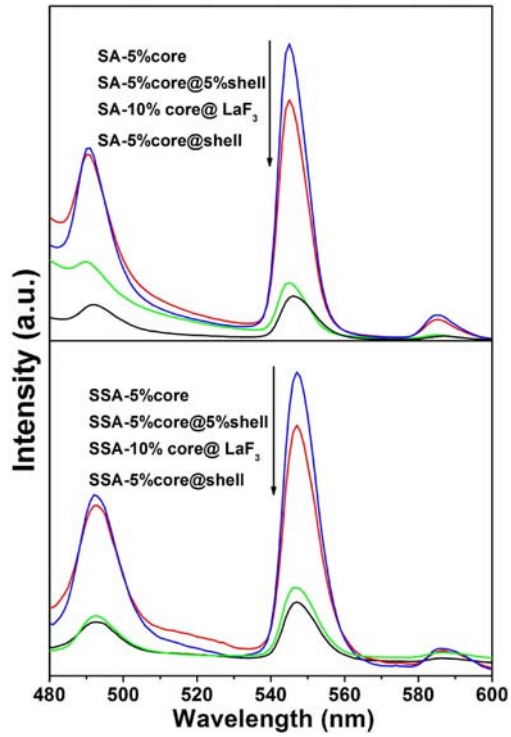

Figure 8 Emission spectra of LaF_3: 10%Tb^{3+} core @ LaF_3 shell, LaF_3: 5%Tb^{3+} core @ LaF_3: 5%Tb^{3+} shell, LaF_3: 5%Tb^{3+} core and LaF_3: 5%Tb^{3+} core @ LaF_3 shell.

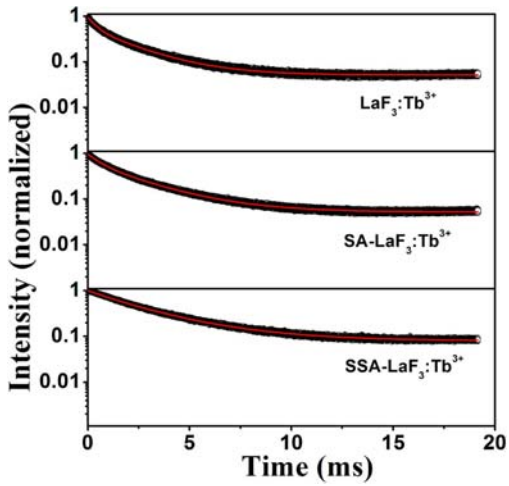

Figure 9 Fluorescent decay curves of the $^5D_4$ – $^7F_5$ transitions of Tb^{3+} at 545 nm ions in LaF_3: 8%Tb^{3+}, SA-LaF_3: 8%Tb^{3+} and SA-LaF_3: 8%Tb^{3+}. The black circles are experimental data, and the red solid lines are fitting functions.

The fluorescence decay curves of Tb^{3+} ions at 545 nm in different samples were measured. Figure 9 shows the representative fluorescence decay curves of Tb^{3+} ions in LaF_3: 8% Tb^{3+} capped with citrate, SA- LaF_3: 8% Tb^{3+} and SA- LaF_3: 8% Tb^{3+}, respectively. All the decay curves are not singly exponential, meaning that the Tb^{3+} ions locate different sites (at the core of the nanoparticles and at or near the surface of nanoparticles, respectively). All of the decay curves are well fitted by a function as $I = I_1 \exp(-\tau_1/t) + I_2 \exp(-\tau_2/t)$, where τ_1 and τ_2 are the

slower and faster decay time constants, respectively. I_1 and I_2 are the proportionality factor of the slower and faster components, respectively. The fitted results for different samples are listed in Table I. The longest component is ascribed to the luminescence decay of Tb^{3+} ions in the core of nanoparticles. It is main contribution to the overall intensity. The shorter component is ascribed to the luminescence decay of Tb^{3+} located at or near the surface of the nanoparticles. The lifetime of Tb^{3+} in the nanoparticles functionalized by aromatic carboxylates are longer than those without functionalization, due to the protection of the ligands molecules (SA or SSA) for Tb^{3+} ions located at or near the surface of the nanoparticles from sources of nonradiative deactivation. The ligands are used not only as sensitizers, but also used to shield the luminescent center ions from high energy oscillators, such as –OH groups in citrate.

Table I. The fluorescence decay lifetime and constant of $^5D_4 \rightarrow {}^7F_5$ transition at 545 nm of Tb^{3+} ions.

Samples	Lifetime (ms)		Ratio constant	
	τ_1	τ_2	I_1	I_2
LaF_3: 1% Tb^{3+}	2.195	0.419	0.56	0.44
LaF_3: 3% Tb^{3+}	2.273	0.422	0.53	0.47
LaF_3: 5% Tb^{3+}	2.435	0.509	0.51	0.49
LaF_3: 8% Tb^{3+}	2.547	0.637	0.53	0.47
LaF_3: 10% Tb^{3+}	2.491	0.551	0.52	0.48
SA-LaF_3: 1% Tb^{3+}	2.385	0.550	0.67	0.33
SA-LaF_3: 3% Tb^{3+}	2.460	0.554	0.63	0.37
SA-LaF_3: 5% Tb^{3+}	2.566	0.590	0.61	0.39
SA-LaF_3: 8% Tb^{3+}	2.604	0.641	0.63	0.37
SA-LaF_3: 10% Tb^{3+}	2.580	0.560	0.60	0.40
SSA- LaF_3: 1% Tb^{3+}	2.735	0.815	0.68	0.32
SSA- LaF_3: 3% Tb^{3+}	2.819	0.858	0.66	0.34
SSA- LaF_3: 5% Tb^{3+}	2. 877	0.974	0.69	0.31
SSA- LaF_3: 8% Tb^{3+}	3.453	1.713	0.66	0.34
SSA- LaF_3: 10% Tb^{3+}	3.223	1.272	0.66	0.34

Conclusions

In summary, LaF_3:Tb^{3+} nanoparticles functionalized by aromatic carboxylates (SA or SSA) have been prepared. The aromatic carboxylates (SA or SSA) can not only extend the excitation wavelength range and greatly enhance the excitation efficiency, but also strongly sensitize the luminescence of Tb^{3+} ions in LaF_3 matrix. The sensitization of aromatic carboxylates for Tb^{3+} is thought to be a short-range effect occurring via a dipole – dipole mechanism. The inorganic LaF_3 shell protects the Tb^{3+} ions from nonradiative deactivation by high energy oscillators, such as –OH groups. It is expected that the organic ligands- functionalized inorganic nanoparticles with a relatively small size have potential applications in light converter for solar cells and bio-analytical field.

Acknowledgements

This project was financially supported by the National Natural Science Foundation of China (NSFC 51172227, 11304021, 51332008), State Key Laboratory of Rare Earth Resource Utilization of Chinese Academy of Sciences (RERU 2013002) and the Science and Technology Development Planning Project of Jilin Province (Grant No. 201205040).

Notes and references

[a] *College of Science, Changchun Institute of Technology, Changchun 130012, P.R. China E-mail: lswen@ciac.jl.cn*
[b] *State Key Laboratory of Rare Earth Resource Utilization, Changchun Institute of Applied Chemistry, Chinese Academy of Sciences, Changchun 130022, P.R. China. Tel: +86 0431 85262031; E-mail: jlin@ciac.ac.cn*

References

1 (a) J.W. Stouwdam, F.C.J.M. van Veggel, *Nano. Lett.* 2002, **2**, 733; (b) S. Heer, O. Lehmann, M. Hasse, H. Güdel, *Angew. Chem. Int. Ed.* 2003, **42**, 3197; (c) M.F. Zhang, H. Fan, B.J. Xi, X.Y. Wang, C. Dong, Y.T. Qian, *J. Phys. Chem. C*, 2007, **111**, 6652.
2 V. sudarsan, F.C.J.M. van Veggel, Rodney A. Herring, M. Raudsepp, *J. Mater. Chem.* 2005, **15**, 1332.
3 K.L. Frindell, M.H. Bartl, A. Popitsch, G.D. Stucky, *Angew. Chem. Int. Ed.* 2002, **41**, 959.
4 Q. Xiao, Y. Liu, L. Liu, R. Li,W. Luo, X. Chen, *J. Phys. Chem. C.* 2010, **114**, 9314.
5 J.W. Stouwdam, M. Raudsepp, F.C.J.M. van Veggel, *Langmuir*, 2005, **21**, 7003.
6 J. Shen, L.D. Sung, J.D. Zhu, L.H. Wei, H.F. Sun, C.H. Yan, *Adv. Funct. Mater.* 2010, **20**, 3707.
7 C. Feldmann, M. Roming, K. Trampert, *Small* 2006, **2**, 1248.
8 X. Zhu, Q. Zhang, Y. Li, H. Wang, *J. Mater. Chem.* 2008, **18**, 5060.
9 Y. Lei, M. Pang, W. Fan, J. Feng, S. Song, S. Dang, H. Zhang, *Dalton Trans.* 2011, **40**, 142.
10 D.M. Yang, X.J. Kang, M.M. Shang, G.G. Li, C. Peng, C.X. Li, J. Lin, *Nanoscale*, 2011, **3**, 2589.
11 J. Wang, J. Hu, D. Tang, X. Liu, Z. Zhen, *J. Mater. Chem.* 2007, **17**, 1597.
12 G. Wang, Q. Peng, Y. Li, *J. Am. Chem. Soc.* 2009, **131**, 14200.
13 J. Zhang, C.M. Shade, D.A. Chengelis, S. Petoud, *J. Am. Chem. Soc.* 2007, **129**, 14834.
14 L.J. Charbonnière, J.L. Rehspringer, R. Ziessel, Y. Zimmermann, *New J. Chem.* 2008, **32**, 1055.
15 A.M. Cross, P.S. May, F.C.J.M. van Veggel, M.T. Berry, *J. Phys. Chem. C.* 2010, **114**, 14740.
16 S. Janssens, G. V. M. Williams, D. Clarke, *J. Appl. Phys.* 2011, **109**, 023506.
17 J.S. Wang, Z.W. Wang, X. Li, S. Wang, H.D. Mao, Z.G. Li, *Appl. Surf. Sci.* 2011, **257,** 7145.
18 Q. Ju, Y.S. Liu, D.T. Tu, H.M. Zhu, R.F. Li, X.Y. Chen, *Chem. Eur. J.* 2011, **17**, 8549.
19 S.W. Li, X. Zhang, Z.Y. Hou, Z.Y. Cheng, P.A. Ma, J. Lin, *Nanoscale*, 2012, **4**, 5619.
20 Y.H. Zheng, X.X. Lin, Q.M. Wang, W.S. Cai, C.C. Zhang, *Mater. Res. Bull.* 2012, **47**, 856.
21 S.W. Li, Z.Y. Hou, Z.Y. Cheng, H.Z. Lian, P.A. Ma, C.X. Li, J. Lin, *RSC Advance*, 2013, **3**, 5491.
22 N. Chen, L. Ju, G.P. Guo, *J. Lumin.* 2014, **153**, 259.
23 S.W. Li, H.J. Ren, S. G. Ju, *J. Nanosci. Nanotech.* 2014, **14**, 3677.
24 J. Lin, Q. Su, *J. Mater. Chem.* 1995, **5**, 1151.
25 K. S. Thomas, S. Singh, G. H. Dieke, *J. Chem. Phys.* 1963, **38**, 2180.
26 Y. Tao, G. W. Zhao, W. P. Zhang, S. D. Xia, *Mater. Res. Bull.* 1997, **32**, 501.